PERGAMON

International Journal of Plasticity 19 (2003) 1377–1400

INTERNATIONAL JOURNAL OF Plasticity

www.elsevier.com/locate/ijplas

An integral elasto-plastic constitutive theory

Zhi-Dong Zhou, She-Xu Zhao, Zhen-Bang Kuang*

Department of Engineering Mechanics, Shanghai JiaoTong University, Shanghai, 200240, PR China

Recieved in final revised form 25th July 2002

Abstract

This paper proposes an integral elasto-plastic constitutive equation, in which it is considered that stress is a functional of plastic strain in a plastic strain space. It is indicated that, to completely describe a strain path, the arc-length and curvature of the trajectory, the turning angles at the corner points and other characteristic points on the path must be considered. In general, the plastic strain space is a non-Euclidean geometric space, hence its measure tensor is a function of not only properties of the material but also the plastic strain history. This recommended integral elasto-plastic constitutive equation is the generalization of Ilyushin, Pipkin, Rivlin and Valanis theories and is suited to research the responses of material under the complex loading path. The predictions of the proposed theory have a good agreement with the experimental results.

Keywords: Plastic strain; Constitutive equation; Non-proportional loading; Delay-angle

1. Introduction

The constitutive equation of a solid is one of the most important properties of material behavior. Modern industry requires higher credibility and nicety of the used structures. Actual engineering structures are generally subjected to non-proportional loading and the constitutive relations under these complex-loading cases are not fully solved. In the last four decades, a lot of authors worked on this area, and with developments of the theory of mechanics, advanced computers and experimental techniques, the constitutive relations of solid material get a fast development and ceaselessly more improvement.

* Corresponding author. Tel.: +86-021-5474-3067; fax: +86-021-6293-3021.
E-mail address: zbkuang@mail.sjtu.edu.cn (Z.-B. Kuang).

0749-6419/03/$ - see front matter
PII: S0749-6419(02)00101-8

In general, plastic constitutive theories have forms in differential, integral and differential–integral cases. Most developments of constitutive equations were in the differential form, while the integral constitutive relations still need to be developed. On the basis of the theories proposed by Hill (1950), Drucker (1950) and Prager (1955), the differential constitutive theories have had a great advancement after the 1970s, especially for complex loading. For example, Besseling (1958) and Mroz (1967) proposed the multisurface model. On the basis of this theory, two-surface plasticity models based on the concept of the bounding surfaces in stress space was proposed (Dafalias and Popov, 1975; Krieg, 1975; Ohno, 1982). The nonlinear kinematic hardening rule was proposed by Armstrong and Frederick (1966) and improved by Chaboche (1977). Recently a set of improved plastic models for metals and composites are proposed (Voyiadjis and Thiagarajan, 1996; Wang and Barkey, 1999; Hashiguchi and Tsutsum, 2001). On the other hand, the kinematic hardening equation with a threshold by Ohno and Wang (1993) can simulate uniaxial ratcheting behavior of metal material. Considering the effect of isotropic hardening, the history effect of mean stress and stress amplitude, Jiang and Sehitoglu (1996a,b) established a better kinematic hardening rule, which could successfully describe uniaxial and multiaxial ratcheting behavior of metal material. Bari and Hassan (2000, 2001, 2002) examined a set of cyclic plasticity models for uniaxial and biaxial ratcheting responses and presented the ratcheting simulation for uniaxial loading that primarily depends on the plastic modulus calculation schemes, whereas, the simulation for multiaxial loading is sensitive to the kinematic hardening rule. In the beginning of the 1950s, for plastic incompressible materials, Ilyushin (1954, 1963) indicated that five-dimensional deviatoric strain and stress vectors spaces are isomorphic and proposed an integral constitutive theory, in which the stress vector may be expressed as a functional of the intrinsic strain space geometry parameters. Subsequently, Lensky (1962) proposed a hypothesis of local definition, which considered that the change of delay angle (the angle between stress vector and strain increment vector) with the strain arc-length is a determinate functional of the delay angle, curvature of the strain path and stress. Later, Pipkin and Rivlin (1965) proposed the "arc-length theory", and Ohashi and Tokuda (1973) and Zubchaninov (1991) carried out a series of experiments and improved this theory. Valanis (1971) proposed the endochronic theory of plasticity, in which the strain arc-length was replaced by intrinsic time to consider the hardening effect caused by plastic strain. Bodner and Partom (1972) constructed a viscoplastic theory. "Unified constitutive theories" were proposed in the mid-1970s to early 1980s for describing inelastic behavior such as creep, relaxation, plasticity, and viscoplasticity (Miller, 1976; Chaboche, 1977; Walker, 1981; Krempl et al., 1986; Shevchenko and Babeshko, 1990; Kaneko and Oyamada, 2000; Lion, 2000; Mahler et al., 2001; Celentano, 2001). These equations are dependent not only on the deformation but also on the time. Marquis (1979), Rousselier et al. (1985), Hashiguchi (1988) and Ohno and Wang (1991) discussed the similarities between different models and showed their equivalence in certain conditions and hypotheses. For example, Chaboche pointed out that the constitutive model developed at ONERA has similarities with other models such as the time-independent model, the unified viscoplastic models by Walker (1981) and Krempl et al. (1986), and the differential form for the

endochronic theory of Valanis (1980). Watanabe and Atluri (1986a,b) discussed that an appropriate choice of the kernel function may result in the multisurface model and the two-surface models. In recent years, the progress in the modeling has been achieved in cooperation with experiments exploring more complicated phenomena (Jiang and Kurath, 1997; Basuroychowdhury and Voyiadjis, 1998; Yoshida, 2000; Zbib and Rubia, 2002).

Kuang (1989, 1990, 2002) constructed a more exact integral constitutive theory, which considered the plastic strain space as a non-Euclidean space and stress to be expressed in the form of Eq. (2) in this paper. Zhao and Kuang (1996a,b), Xiao and Kuang (1998), Zhou and Kuang (1999) carried out a series of axial-torsional combined loading experiments and theoretical analyses. They obtained some basic rules, such as approximate expressions about stress norm and delay angle with the change of strain path and its turning angle etc. Based on the previous results, this paper proposes some new rules and gives the evolution equations of parameters included in the integral constitutive equation. It is also shown that the predictions by this theory are in agreement with the experimental results.

2. An integral constitutive theory

According to the Ilyushin theory, it is assumed that the strain space, plastic strain space and stress space are isomorphic and can be indicated in the same space with their own scales. In these spaces, a deformation process can be described through a corresponding curve and some characteristic points. The geometrical form of a curve in n-dimensional space can be described entirely by intrinsic arc-length z, curvature vector $\boldsymbol{\kappa}$ ($\boldsymbol{\kappa}$ has $n-1$ components) and some characteristic points. In a plastic strain space, the characteristic points are starting point, corner point (where the direction of plastic strain rate changes) or the point where plastic strain norm reaches maximum value (considering the effect of memory or over loading). To consider the effect of the plastic strain history on material property, the plastic strain space is regarded as a non-Euclidean space that has the measure tensor $\mathbf{T}$. We may call the differential arc-length in non-Euclidean strain space as differential intrinsic time or endochronic (this terminology in plasticity is first introduced by Valanis, 1971), which is defined by

$$\mathrm{d}z = \sqrt{\mathrm{d}\boldsymbol{\varepsilon}^p : \mathbf{T} : \mathrm{d}\boldsymbol{\varepsilon}^p}, \qquad z = \int \mathrm{d}z \tag{1}$$

where $\mathbf{T}$ is a function of material behavior and functional of plastic strain history, which may be related to material microscopic structures and their evolutions. This indicates that the plastic strain space is different from the usual geometric non-Euclidean space. So the endochronic is monotonously increasing, and this property is analogous to time. The general form of integral elasto-plastic constitutive equation is recommended by Kuang (1989, 1990, 2002)

$$\boldsymbol{\sigma} = \int_0^{\zeta} F(\zeta, z, \boldsymbol{\kappa}(z), z_i)\mathrm{d}\boldsymbol{\varepsilon}^p(z) \tag{2}$$

where $\boldsymbol{\sigma}$ and $\boldsymbol{\varepsilon}^p$ are stress vector and plastic strain vector respectively, the variable ζ is the current value of endochronic; and z_i is the intrinsic time corresponding to the ith characteristic point.

For isotropic hardening materials, $\mathbf{T}$ can be described by

$$\mathbf{T} = \mathbf{I}/f^2(L) \tag{3}$$

$$T_{ij} = \delta_{ij}/f^2(L), \qquad \mathrm{d}L^2 = \mathrm{d}\boldsymbol{\varepsilon}^p \cdot \mathrm{d}\boldsymbol{\varepsilon}^p \tag{4}$$

where $\mathbf{I}$ denotes the identity tensor, δ_{ij} is the Kronecker delta, L is the accumulated plastic strain arc-length in the usual sense, and $f(L)$ is the isotropic hardening function. In order to simplify the practical calculation, here we use L, not z, in Eqs. (3) and (4).

By introducing normalized plastic strain $\bar{\boldsymbol{\varepsilon}}^p$

$$\mathrm{d}\bar{\boldsymbol{\varepsilon}}^p = \mathrm{d}\boldsymbol{\varepsilon}^p/f(L) \tag{5}$$

one can obtain

$$\mathrm{d}z^2 = \mathrm{d}\bar{\boldsymbol{\varepsilon}}^p \cdot \mathrm{d}\bar{\boldsymbol{\varepsilon}}^p = \left(\mathrm{d}L^2\right)/f^2(L) \tag{6}$$

To do so, the arc-length of normalized plastic strain space is Euclidean space when $\mathbf{T}$ is expressed by Eq. (3).

For plastic incompressible material, the plastic strain vector only has five independent components, which constructs a five-dimensional space. Let $\mathbf{q}_i$ ($i = 1, 2, 3, 4, 5$) be the orthogonal base vectors of the five-dimensional space, plastic strain vector, stress vector and their rate can be expressed as

$$\boldsymbol{\varepsilon}^p = \varepsilon_i^p \mathbf{q}_i, \quad \dot{\boldsymbol{\varepsilon}}^p = \dot{\varepsilon}_i^p \mathbf{q}_i, \quad \boldsymbol{\sigma} = \sigma_i \mathbf{q}_i, \quad \dot{\boldsymbol{\sigma}} = \dot{\sigma}_i \mathbf{q}_i \tag{7}$$

where ε_i^p and σ_i are the components in plastic strain and stress vector projecting on base vector $\mathbf{q}_i$ respectively. The upper dot denotes differentiation with respect to the real time.

Let $\mathbf{e}$ and $\mathbf{S}$ denote deviatoric stain tensor and stress tensor respectively and e_{kl} and S_{kl}($k,l = 1, 2, 3$) are their components. Following Ilyushin, the relations between ε_i and e_{kl} are written as

$$\begin{aligned} &\varepsilon_1 = e_{11}, \qquad \varepsilon_2 = (e_{11} - 2e_{22})/\sqrt{3} \\ &\varepsilon_3 = 2e_{12}/\sqrt{3}, \quad \varepsilon_4 = 2e_{23}/\sqrt{3}, \quad \varepsilon_5 = 2e_{31}/\sqrt{3} \end{aligned} \tag{8}$$

Similarly, the relation between σ_i and S_{kl} are

$$\begin{aligned} &\sigma_1 = 3S_{11}/2, \quad \sigma_2 = \sqrt{3}(S_{11} + 2S_{22})/2 \\ &\sigma_3 = \sqrt{3}S_{12}, \quad \sigma_4 = \sqrt{3}S_{23}, \quad \sigma_5 = \sqrt{3}S_{31} \end{aligned} \tag{9}$$

For isotropic and incompressible material, we define plastic delay angle θ (θ^p) with plastic strain trajectory as

$$\cos\theta = \frac{\mathrm{d}\boldsymbol{\varepsilon}^p \cdot \boldsymbol{\sigma}}{|\mathrm{d}\boldsymbol{\varepsilon}^p||\boldsymbol{\sigma}|}$$

$$|\boldsymbol{\sigma}| = \sqrt{\boldsymbol{\sigma}\cdot\boldsymbol{\sigma}}, \quad |\mathrm{d}\boldsymbol{\varepsilon}^p| = \sqrt{\mathrm{d}\boldsymbol{\varepsilon}^p\cdot\mathrm{d}\boldsymbol{\varepsilon}^p} \tag{10}$$

where $|\boldsymbol{\sigma}|$ and $|\mathrm{d}\boldsymbol{\varepsilon}^p|$ are the equivalent stress and the equivalent plastic strain increment.

3. Axial-torsional combined loading case

3.1. Basic equation

Because of the multiformity of materials and loading path, it is very difficult to describe the constitutive function for a general deformation trajectory in the five-dimensional plastic strain space. In fact, the external load for common engineering structures can be approximated with combining some simple loading histories and most of the test machines are designed with axial-torsional combined loading system for complex loading experiments. So the research work in literatures are mainly on axial-torsional combined loading.

Fig. 1 shows a plastic deformation path in two-dimensional normalized plastic strain space $\bar{\varepsilon}_1^p - \bar{\varepsilon}_3^p$ with base vectors $\mathbf{q}_1$ and $\mathbf{q}_3$. $\mathbf{P}_1$ and $\mathbf{P}_3$ denote natural base vectors in a local nature coordinate system at a point on the plastic strain trajectory, where $\mathbf{P}_1$ is along the tangential direction and $\mathbf{P}_3$ is along the normal direction of the plastic strain path. When $\mathbf{P}_1$ and $\mathbf{P}_3$ construct a right-hand coordinate system, we have

$$\begin{aligned} &\mathrm{d}\bar{\boldsymbol{\varepsilon}}^p = \mathrm{d}\bar{\varepsilon}_1^p\mathbf{q}_1 + \mathrm{d}\bar{\varepsilon}_3^p\mathbf{q}_3 = \mathrm{d}z\mathbf{P}_1, \quad \varepsilon_3 = \gamma/\sqrt{3} \\ &\boldsymbol{\sigma} = \sigma_1\mathbf{q}_1 + \sigma_3\mathbf{q}_3, \quad \sigma_3 = \sqrt{3}\tau, \quad \mathrm{d}z = \sqrt{\left(\mathrm{d}\bar{\varepsilon}_1^p\right)^2 + \left(\mathrm{d}\bar{\varepsilon}_3^p\right)^2} \end{aligned} \tag{11}$$

where τ and γ are shear stress and engineering shear strain respectively.

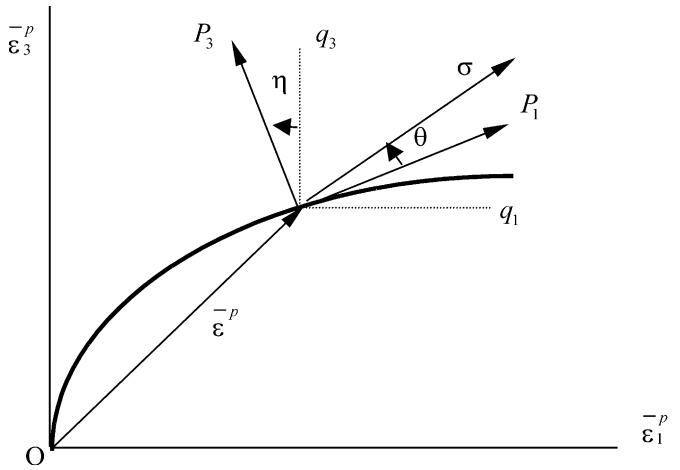

Fig. 1. The plane (plastic) strain space.

In a general five-dimensional plastic strain space, according to the Serret–Frenet's formula we have

$$\frac{\mathrm{d}\mathbf{P}_n}{\mathrm{d}z} = -\kappa_{n-1}\mathbf{P}_{n-1} + \kappa_n\mathbf{P}_{n+1}, \quad n = 1,2,3,4,5,6$$
$$\kappa_0 = \kappa_6 = 0, \quad \mathbf{P}_0 = \mathbf{P}_7 = 0 \tag{12}$$

where κ_n is curvatures of deformation trajectory, $\mathbf{P}_n$ is local natural coordinate on the curve of deformation path. In two-dimensional normalized plastic strain space, Eq. (12) is degenerated to

$$\frac{\mathrm{d}\mathbf{P}_1}{\mathrm{d}z} = \bar{\kappa}\mathbf{P}_3, \qquad \frac{\mathrm{d}\mathbf{P}_3}{\mathrm{d}z} = -\bar{\kappa}\mathbf{P}_1 \tag{13}$$

where $\bar{\kappa}$ is relative curvature of the plastic strain path. If $\mathbf{P}_3$ point to the curvature center of the plastic strain path, $\bar{\kappa}$ takes positive value; conversely $\bar{\kappa}$ takes negative value. According to Eq. (10), one gets

$$\cos\theta = \frac{\boldsymbol{\sigma}\cdot\mathrm{d}\bar{\boldsymbol{\varepsilon}}^p}{|\boldsymbol{\sigma}|\mathrm{d}z} \tag{14a}$$

$$\boldsymbol{\sigma} = \sigma(\cos\theta P_1 + \sin\theta P_3) \tag{14b}$$

where σ denotes stress norm. Differentiating Eq. (14b) with respect to z, and using Eq. (13), one obtains

$$\dot{\boldsymbol{\sigma}} = \bar{g}_1\mathbf{P}_1 + \bar{g}_3\mathbf{P}_3$$
$$\bar{g}_1 = \dot{\sigma}\cos\theta - \sigma\left(\bar{\kappa} + \dot{\theta}\right)\sin\theta, \quad \bar{g}_3 = \dot{\sigma}\sin\theta + \sigma\left(\bar{\kappa} + \dot{\theta}\right)\cos\theta \tag{15}$$

Let η be the angle between $\mathbf{q}_1$ and $\mathbf{P}_1$ (Fig. 1), using

$$\cos\eta = \frac{\mathrm{d}\bar{\varepsilon}_1^p}{\mathrm{d}z}\frac{\mathrm{d}\varepsilon_1^p}{\mathrm{d}L}, \qquad \sin\eta = \frac{\mathrm{d}\bar{\varepsilon}_3^p}{\mathrm{d}z} = \frac{\mathrm{d}\varepsilon_3^p}{\mathrm{d}L} \tag{16}$$

and the transformation relation of two coordinate systems, one obtains

$$\begin{Bmatrix} \mathrm{d}\sigma_1 \\ \mathrm{d}\sigma_3 \end{Bmatrix} = \begin{bmatrix} \bar{g}_1 & -\bar{g}_3 \\ \bar{g}_3 & \bar{g}_1 \end{bmatrix} \begin{Bmatrix} \mathrm{d}\bar{\varepsilon}_1^p \\ \mathrm{d}\bar{\varepsilon}_3^p \end{Bmatrix} \begin{bmatrix} g_1 & -g_3 \\ g_3 & g_1 \end{bmatrix} \begin{Bmatrix} \mathrm{d}\varepsilon_1^p \\ \mathrm{d}\varepsilon_3^p \end{Bmatrix}$$

$$g_i = \bar{g}_i/f(L); \quad i = 1,3 \tag{17}$$

Eq. (17) is the basic constitutive equation for axial-torsional combined loading. It reflects naturally the fact that the plastic response is dependent on the intrinsic geometry parameters and plastic delay angle θ. The stresses are dependent on all strain components. Here $\dot{\boldsymbol{\sigma}}$ plays the role of "plastic modulus", and $\dot{\theta}$ plays the role of

"rate of non-proportional measure". For the proportional loading condition, there is $\theta = \dot{\theta} = \bar{\kappa} = 0$, so Eq. (17) is reduced to

$$d\sigma_1 = \dot{\sigma} d\bar{\varepsilon}_1^p = \frac{d\sigma_1}{dL} d\varepsilon_1^p, \quad d\sigma_3 = \dot{\sigma} d\bar{\varepsilon}_3^p = \frac{d\sigma}{dL} d\varepsilon_3^p \tag{18}$$

In this case, the present theory is equivalent to Valanis's endochronic theory.

3.2. Experiment procedure and establishment of variation rules of θ and σ

In the aspect of integral constitutive equation, Lensky (1962), Mashkov (1970), Ohashi and Tokuda (1973) and Zhao and Kuang (1996a) finished their experiments under the axial-torsional loading cases. In the experiment of Zhao and Kuang (1996a), material selected for this study is the 1Cr18Ni9Ti stainless steel whose chemical composition is shown in Table 1 and the Young's modulus and shear modulus are determined as $E = 205$ GPa and $G = 77$ GPa respectively. After the specimen is machined roughly, it is annealed (furnace cooled after soaking at 1050 °C for 40 min) to obtain a initial isotropy of the material. Tubular specimens with outside diameter of 25 mm, wall thickness of 2 mm and gauge length of 25 mm, shown in Fig. 2, are finished carefully.

An MTS809 servo-controlled electro-hydraulic testing machine is used in the experiments. All experiments are conducted under strain control axial-torsional combined loads with the aid of a computer system for control and data acquisition. The effective strain rate of 5×10^{-14} s^{-1} was selected for the loading processes. The values of axial and shear strain components in the specimen are measured by using an MTS (25 mm) clip gauge axial-torsional extensometer clipped on the gauge section. The various strain paths in the vector space (ε_1–ε_3) used in experiments are shown in Fig. 3. The strain paths are consisted of three linear segments, circular or elliptical segments.

Table 1
Chemical composition of 1Cr18Ni19Ti

Chemical composition	C	Mn	Si	Cr	Ni	P	Ti	S	Fe
Weight percentage (%)	0.10	1.60	0.80	18.00	8.0	0.035	0.58	0.03	The rest

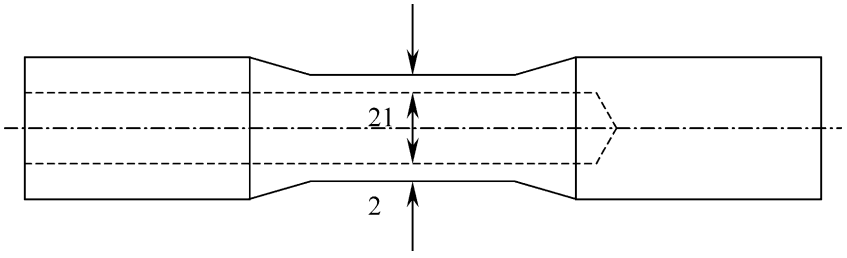

Fig. 2. Thin-walled tubular specimen.

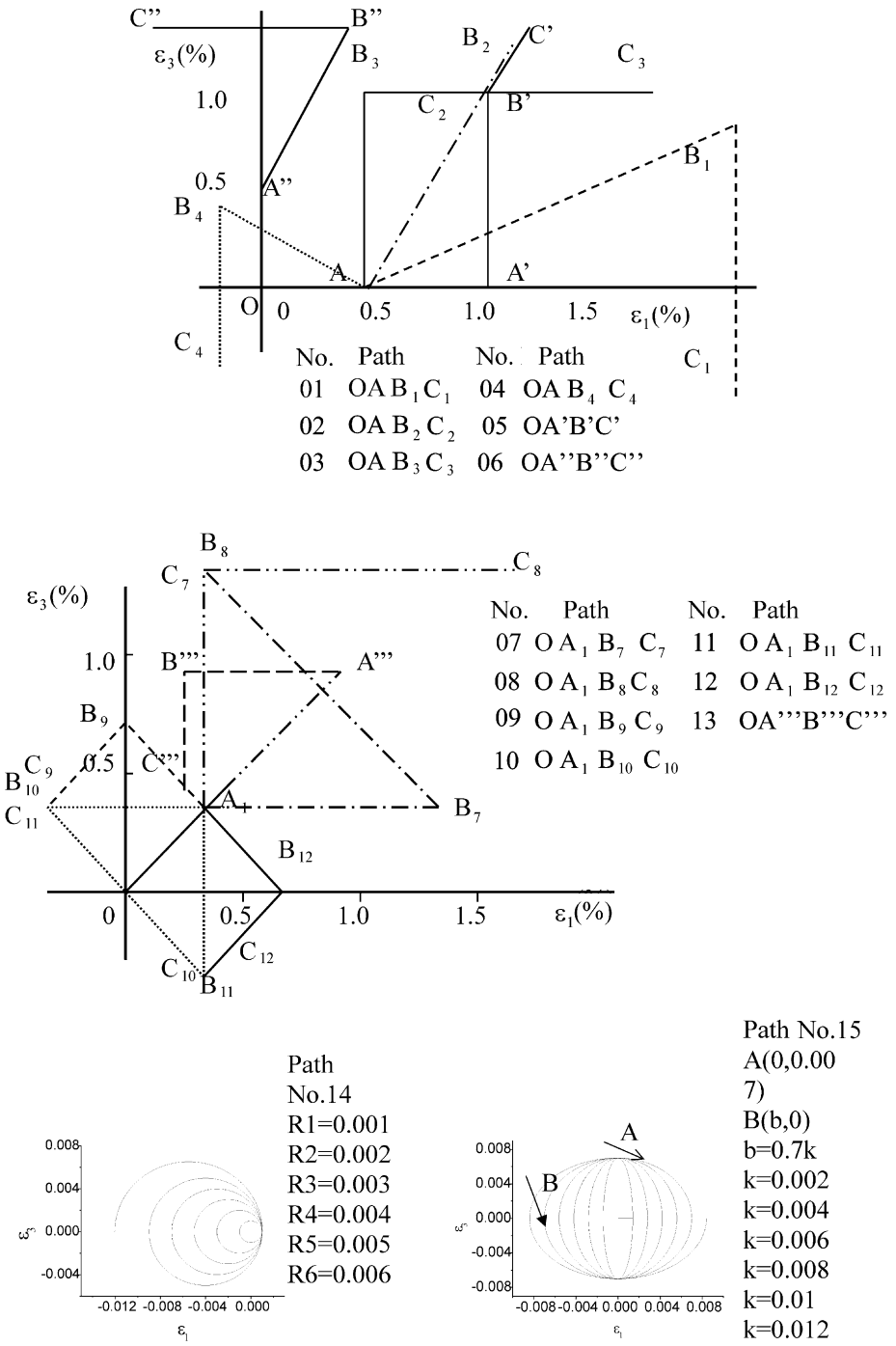

Fig. 3. Strain path in the experiment.

3.2.1. Evolution equation of delay angle θ

When the direction of plastic strain path changes, stress vector will not be immediately aligning with plastic strain increment vector, i.e. the response of material appears delay phenomenon. Plastic delay angle θ is a function of the loading history and the intrinsic geometry parameters of strain path.

(1) For some multi-segment linear strain paths, plastic strain is $\boldsymbol{\varepsilon}^p = \mathbf{e} - \mathbf{S}/2G$ (G is shear modulus and $\mathbf{S}$ is deviatoric stress). Fig. 4 shows the change of plastic delay angle θ with the increment of the plastic trajectories $\Delta l^p (= l^p - l_0^p)$ in the second linear segment where l_0^p is the plastic strain length at the beginning of the second linear segment. These paths have the same pre-strain length l_0^p but the angles α_0 between ε_1 and $\boldsymbol{\varepsilon}$ are different. From Fig. 4, one concludes that the plastic delay angle θ at the corner is slightly smaller than turning angle α of the path. With Δl^p increasing, θ gradually approaches to zero in exponential rule, on the other words, stress vector and strain increment vector will almost have the same direction when plastic deformation is large enough. The larger the value of α, the rapider the attenuation of θ at the initial stage of Δl^p. If plastic strain yield function is used to describe loading and unloading (Naghdi and Trapp, 1975), the boundary of loading and unloading is given by

$$\left(\varepsilon_1 - \varepsilon_1^p\right)\mathrm{d}\varepsilon_1 + \left(\varepsilon_3 - \varepsilon_3^p\right)\mathrm{d}\varepsilon_3 = 0 \tag{19}$$

If the loading is proportional before the corner, Eq. (19) indicates that plastic strain increment is almost perpendicular to previous plastic strain path. This means that it is loading when $\alpha < 90^\circ$ and unloading when $\alpha > 90^\circ$. Fig. 4 also shows that

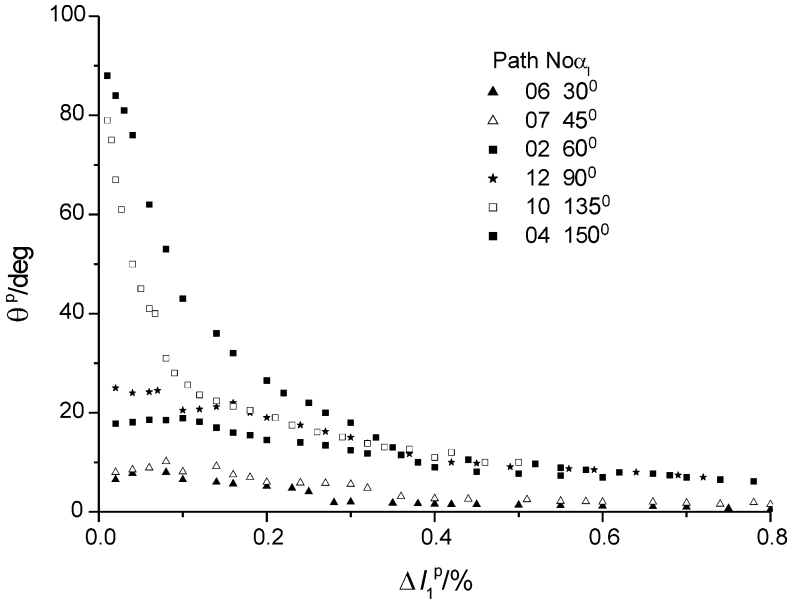

Fig. 4. Variation of delay angle with the length of strain path after turning point (equal pre-strain, different turning angle).

the curve $\theta-\Delta l^p$ can be expressed by a unique equation in the case of $\alpha<90^\circ$ and another equation in the case of $\alpha>90^\circ$. While for reverse loading, namely $\alpha=180^\circ$, θ will decrease from 180° to zero very rapidly.

According to the experiments in literature and results shown in Fig. 4, the exponent functions may be suitable to describe the variation of plastic delay angle under multi-segment linear loading strain paths. By the discussion cited above, plastic delay angle along the ith segment is described by

$$\theta=\begin{cases} d_1\alpha e^{-B_1(\zeta-z_{i-1})} & |\alpha|\leqslant\pi/2 \\ d_2\alpha e^{-B_2(\zeta-z_{i-1})} & |\alpha|>\pi/2 \end{cases} \tag{20}$$

where d_1, d_2, B_1 and B_2 are material constants, and $z_{i\text{-}1}$ denotes the intrinsic time at beginning of ith segment.

(2) To see the influence of the arc-length of (i-1)th segment on plastic delay angle θ along the ith segment, Figs. 5 and 6 give the relations of θ and Δl^p along the third linear segment. The turning angles from the second segment to third segment are $\alpha=90^\circ$ and $\alpha=135^\circ$ respectively. These two Figures show that in all cases when the second segment length achieves a certain value (about 0.8–1.0% in our experiments), the change of θ versus Δl^p along the third segment has almost the same rule as that along the second segment. Conversely, if the second segment length is not large enough, θ is not equal to zero at the end of the second segment and the curve $\theta-\Delta l^p$ along the third segment is obviously higher than that along the second segment. This means the relation of θ and Δl^p in these cases can still be described by Eq. (20), but a

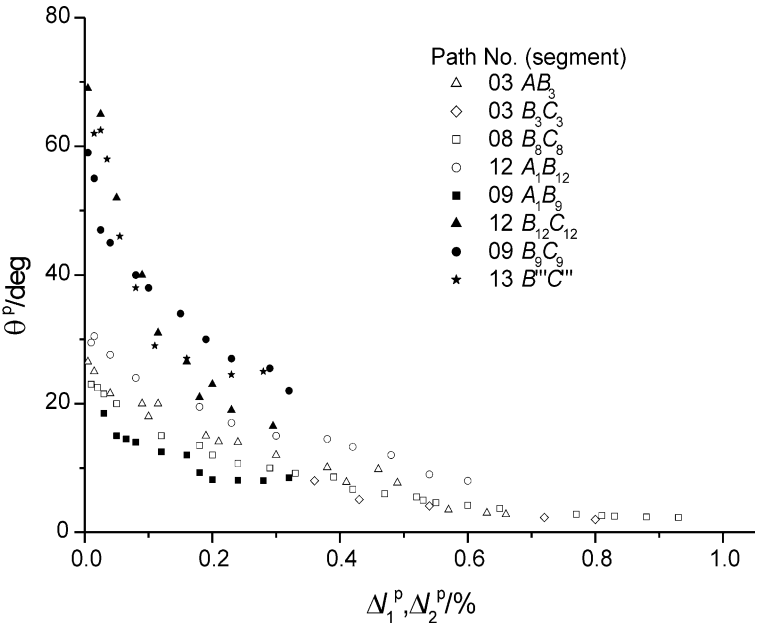

Fig. 5. Variation of delay angle with the length of strain path after turning point (equal turning angle, different preceding strain history).

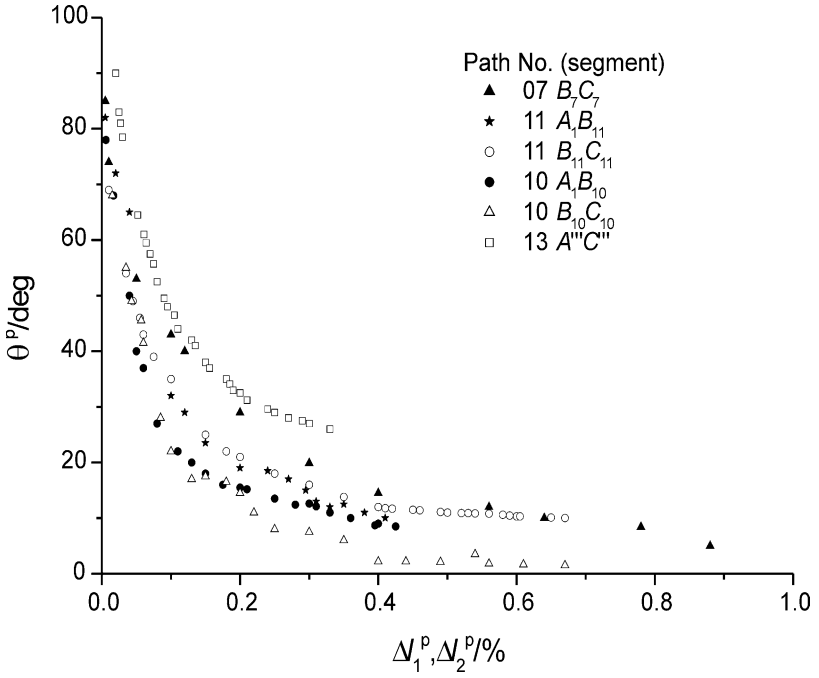

Fig. 6. Variation of delay angle with the length of strain path after turning point (equal turning angle, different preceding strain history).

remnant delay angle θ_d computed at the end of $(i-1)$th segment should be added to α, that is

$$\alpha = \begin{cases} |\theta_d \pm \alpha| & |\theta_d \pm \alpha| \leqslant \pi \\ 2\pi - |\theta_d \pm \alpha| & |\theta_d \pm \alpha| > \pi \end{cases} \tag{21}$$

(3) For some smooth curve strain paths, the variation of plastic delay angle θ depends not only on curvature κ, but also on the rate of curvature $\dot{\kappa}$. The variation of θ with curvature κ is investigated through changing the radii of the circular paths. It is found that θ is constant along a circular path with a constant radius. Fig. 7 shows the change of θ with κ. It can be seen that θ increases with increasing κ. In general, the relation of θ and κ can be approximated with a straight line which does not pass the origin when curvature is not small.

For the elliptical strain path depicted in Fig. 3, the variation of θ with κ can be discovered through changing the ratio of major axis to minor axis of the ellipse. Fig. 8 shows the variation of θ with Δl^p along the elliptical strain path. When curvature κ decrease, θ is decreasing with growing Δl^p.

From Figs. 7 and 8, plastic delay angle θ can be expressed by a power function of curvature and a attenuation function of the plastic strain arc-length. The approximate expression of θ for the ith segment can be written as

$$\theta = d_4\kappa^m + d_3\left(\dot{\kappa}/|\dot{\kappa}|\right)e^{-(\zeta - z_{i-1})} \tag{22}$$

where d_3, d_4 are material constants.

3.2.2. Evolution equation of stress norm

When the direction of plastic strain rate changes, stress vector has an abrupt drop in a very short range at subsequent path due to softening of material. Later, it resumes hardening again with increasing of plastic deformation.

Fig. 9 (Zhao and Kuang, 1996a) depicts the change of $\bar{\sigma} = |\boldsymbol{\sigma}|/|\boldsymbol{\sigma}_c|$ ($\boldsymbol{\sigma}_c$ denotes stress vector at the corner point) with the plastic strain arc-length Δl^p. The results show that the drop of the magnitude of stress vector can be expressed as a function of turning angle α at the corner point and the drop of $\bar{\sigma}$ will increase with increasing α. When α is less than 60°, this drop is not obvious and the subsequent hardening curve is almost coincided with the curve without turn. When α is about 90°, namely stress vector $\boldsymbol{\sigma}$ and plastic strain rate $\dot{\boldsymbol{\varepsilon}}^p$ are almost perpendicular, the drop is significant and the subsequent hardening curve is slightly higher than the curve without turn. And when α is larger than 90°, the drop and subsequent hardening are more obvious. For simplicity, we may approximatively consider that the stress has no drop when $\alpha < 90°$.

The change of material properties responding to external load is the results of the change of microscopic structure within material. The experimental observations show that the spatial dislocation structures such as nervation, wall-structure, labyrinthic structure and cystiform structure etc. are formed under plastic deformation. The strong non-linear coupling and interaction between dislocations lead to the instability and forks of distributing state of dislocations, which form the non-balanced self-organized structure (Mughrabi et al., 1979; Dewel et al., 1981). In

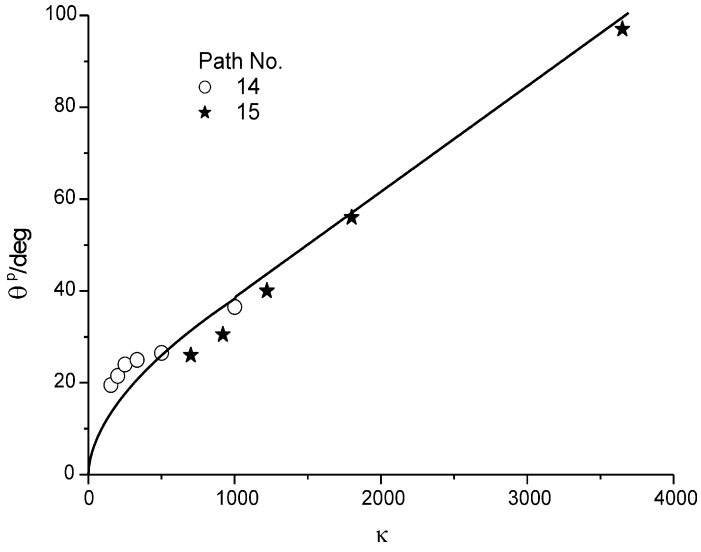

Fig. 7. Variation of delay angle with the curvature of (plastic) strain path.

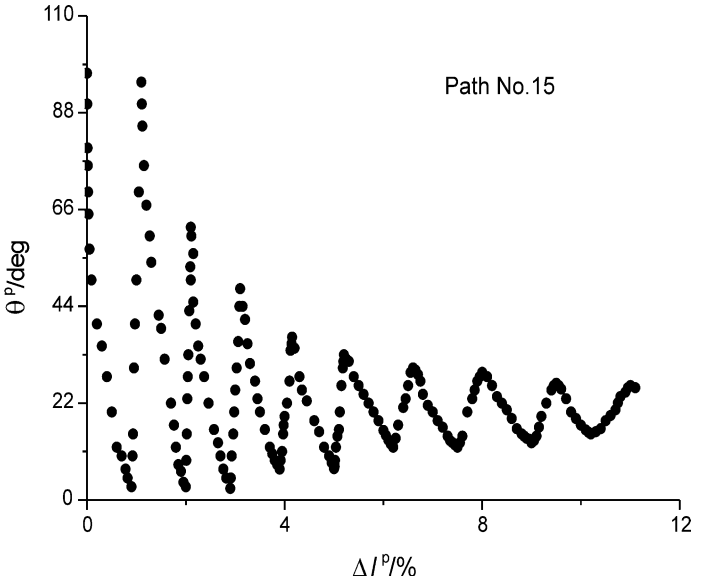

Fig. 8. Variation of delay angle with the length of (plastic) strain path for path 15.

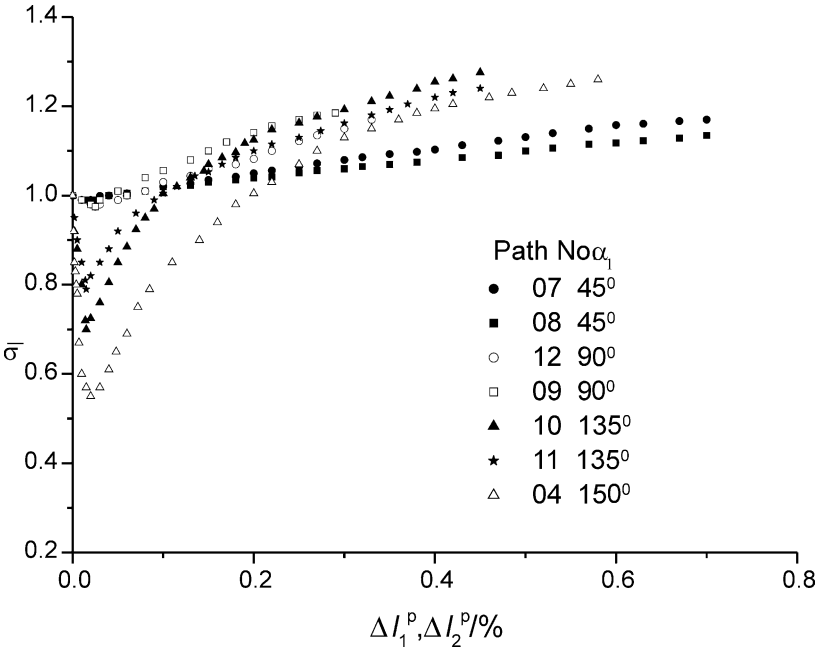

Fig. 9. Variation of the magnitude σ with Δl^p(equal pre-strain, different turning angle).

loading condition, dislocations happen to accumulate and bow out in front of the stress field of the crystallitic boundary, the sub-crystallitic boundary and some inclusions. After the change of direction of loading path, the maximum shear stress plan happens to rotate and internal stress that caused the previous dislocation accumulation releases gradually, moreover new slippage systems actuate gradually, which lead to the drop of stress in a macroscopic scale. Subsequently, with increasing of the deformation, new dislocation structures within material form gradually and material shows the hardening resumption in the macroscale.

Based on the J_2 flow theory, Zhou and Kuang (1999) analyzed the plane stress problem for two phases material subjected to bi-axial tension with elasto-plastic FEM. They also found the above phenomena, plastic delay angle θ can be described by Eqs. (20) and (21) and the drop of stress norm can be expressed as

$$\frac{\Delta\sigma}{\sigma_c}\times 100=\begin{Bmatrix}(8.2682-0.10149\alpha)^2 & \alpha>81.468^\circ\\ 0 & \alpha<81.468^\circ\end{Bmatrix} \tag{23}$$

where σ_c is the flow stress. According to the analysis, the calculational results for two-phase material have the same qualitative features as the results using integral constitutive equation that will be discussed later.

The above investigations show that the response of material to external load is closely connected with the intrinsic geometry parameters of loading path and the effect of the past history of plastic strain on the present response is attenuated. Hence, σ can be approximately given by

$$\sigma=\sigma(\zeta,z,\bar{\kappa}(z))=\sigma(\zeta-z,\kappa(L)),\quad \kappa=\bar{\kappa}/f(L)$$

or concretely by

$$\sigma(\zeta-z,\kappa(L))=f(L)\sum_{\rho=1}^{N}\frac{R_\rho}{A_\rho}e^{-A_\rho(\zeta-z)},\quad A_\rho=A_\rho(z,\kappa) \tag{24}$$

where κ is the curvature of the two-dimensional plastic strain trajectory, R_ρ and A_ρ are material constants.

3.3. Constitutive equation for axial-torsional combined loading

In axial-torsional combined loading, the integral constitutive Eq. (2) is degenerated to the constitutive equation in the two-dimensional plastic strain space. Substituting Eq. (24) into Eq. (15) and neglecting small terms in high order, then

$$\begin{Bmatrix} g_1=\sum_{\rho=1}^{3}R_\rho N_\rho e^{-A_\rho(\zeta-z)} & N_\rho\approx\cos\theta-f(L)\sin\theta\left(\kappa+\frac{\mathrm{d}\theta}{\mathrm{d}L}\right)/A_\rho\\ g_3=\sum_{\rho=1}^{3}R_\rho M_\rho \mathrm{e}^{-A_\rho(\zeta-z)} & M_\rho\approx\sin\theta+f(L)\cos\theta\left(\kappa+\frac{\mathrm{d}\theta}{\mathrm{d}L}\right)/A_\rho\end{Bmatrix} \tag{25}$$

Substituting the above equation into Eq. (17) and integrating it, one obtains

$$\begin{Bmatrix} \sigma_1 \\ \sigma_3 \end{Bmatrix} = \sum_{\rho=1}^{3} \int_0^{\zeta} R_\rho e^{-A_\rho(\zeta - z)} \begin{bmatrix} N_\rho & -M_\rho \\ M_\rho & N_\rho \end{bmatrix} \begin{Bmatrix} \mathrm{d}\varepsilon_1^p \\ \mathrm{d}\varepsilon_3^p \end{Bmatrix} \tag{26}$$

where plastic delay angle θ is determined by Eqs. (20), (21) and (22).

The experimental results show that hardening behavior of materials with growing plastic strain has a trend to saturation whether in proportional or non-proportional loading. Hence, $f(L)$ has the saturated form and can be approximately given by

$$f(L) = C_0 - (C_0 - 1)e^{-hL} \tag{27}$$

where C_0 and h are material constants.

4. Analysis of strain-controlled axial-torsional combined test

As the application, we use Eq. (26) to simulate stress response of the 1Cr18Ni19Ti stainless steel in the strain-controlled axial-torsional test.

4.1. The method to determine parameters

There need 15 material constants grouped to three kinds to describe this test. The first kind of constants A_1, A_2, A_3, R_1, R_2 and R_3 reflect the memory effect of material including; the second kind of constants d_1, d_2, d_3, d_4, B_1, B_2 and m reflect the change of plastic delay-angle θ with the plastic strain path including; the third kind constants C_0 and h reflect the isotropic hardening including.

(1) The determination of constants A_1, A_2, A_3, R_1, R_2, R_3, C_0 and h. According to the above discussion, integral constitutive equation is reduced to Valanis's endochronic equation under proportional loading. In this case, plastic delay-angle θ, the rate of θ and curvature κ are all zero, except at the reverse point in reverse loading. Hence, the material parameters can be determined using the cyclic hysteresis loop of the torsional loading when the length of straight trajectory is not less than the saturated length. Due to $\theta = \dot{\theta} = \kappa = 0$, $N_\rho = 1$ and $M_\rho = 0$, Eq. (26) gives

$$\sigma_3 = \sum_{\rho=1}^{3} \int_0^{\zeta} R_\rho e^{-A_\rho(\zeta - z)} \mathrm{d}\varepsilon_3^p \tag{28}$$

When $L \to \infty$, from Eq. (27), there is approximatively $f(L) = C_0$. When $L = 0$, there is $f(L) = 1$. Hence, the hardening function $f(L)$ changes from 1 to C_0 when plastic strain arc-length L from $0 \to \infty$.

On the cyclic hysteresis loop, suppose $Q-1$ and Q as the starting point and end point of the Qth straight segment of the plastic strain path. For the Qth loading path, there is

$$\sigma_3 = \sum_{i=1}^{Q-1}\sum_{\rho=1}^{3}(-1)^{i-1}\int_{Z_{i-1}}^{Z_i} R_\rho e^{-A_\rho L_i(\zeta-z)}\mathrm{d}\varepsilon_3^p + \sum_{\rho=1}^{3}(-1)^{Q-1}\int_{Z_{Q-1}}^{\zeta} R_\rho e^{-A_{\rho Q}(\zeta-z)}\mathrm{d}\varepsilon_3^p \quad (29)$$

When $z_0=0$, the sub-index i expresses the ith corner point on the path. Applying linear approximate expression

$$Z_{i+1} - Z_i = (L_{i+1} - L_i)/f_i \quad (30)$$

where f_i is the value of the hardening function at the ith point, $(\zeta-z)$ can be expanded as

$$\zeta - z = \frac{l - L_{Q-1}}{f_{Q-1}} + \frac{L_{Q-1} - L_{Q-2}}{f_{Q-2}} + \cdots\cdots + \frac{L_{i+1} - L_i}{f_i} + \frac{L_i - L}{f_{i-1}} \quad (31)$$

Substitute Eq. (31) into Eq. (28) and integrate it. Considering $A_{\rho i}\approx A_\rho, f_i\approx C_0$ in the saturated state and neglecting small terms in high order, one obtains

$$\begin{cases} \sigma_3 = \sum_{\rho=1}^{3} R_\rho(-1)^{Q-1}\dfrac{C_0}{A_\rho}\left[1-\left(1-(-1)^{Q-1}T_\rho\right)e^{-A_\rho\left(l-L_{Q-1}\right)/C_0}\right] \\ T_\rho = (-1)^{Q-2}\left(1-2e^{-A_\rho\left(L_{Q-1}-L_{Q-2}\right)/C_0}\right) \end{cases} \quad (32)$$

In the new coordinate system $(\tilde{\varepsilon}_3^p, \tilde{\sigma}_3^p)$ (Yanagida and Watanabe, 1991), Eq. (32) is reduced to

$$\begin{cases} \sigma_3 = \sum_{\rho=1}^{3} R_\rho \dfrac{C_0}{A_\rho}\left(1-T_\rho\right)\left(1-e^{-A_\rho\tilde{\varepsilon}_3^p/C_0}\right) = \sum_{\rho=1}^{3} D_\rho\left(1-e^{-H_\rho\tilde{\varepsilon}_3^p}\right) \\ T_\rho = 2\mathrm{e}^{-A_\rho\Delta\varepsilon_3^p/C_0} - 1 \end{cases} \quad (33)$$

where $\Delta\varepsilon_3^p(=\varepsilon_{3(i)}^p - \varepsilon_{3(i-1)}^p)$ is the range of plastic strain.

By simulating the experiments with Eq. (33), one obtains D_ρ and H_ρ. Therefore, A_ρ/C_0 and R_ρ can be determined by

$$A_\rho/C_0 = H_\rho, \quad R_\rho = \frac{D_\rho H_\rho}{2\left(1-e^{-H_\rho\Delta\varepsilon_3^p}\right)} \qquad (\rho = 1, 2, 3) \quad (34)$$

Using the saturated cyclic hysteresis loop is more reasonable than the axial tension curve to determine constants of hardening function. In initial segments corresponding to monotonous torsional loading and following reverse loading, the hardening function can be expressed as a linear form due to small plastic strain arc-length. Namely, suppose

$$f'(L) = 1 + h'L \quad (35)$$

For the initial monotonous loading segment, substituting Eqs. (28) into (35), one obtains

$$\sigma_3 = \sum_{\rho=1}^{3} \frac{R_\rho}{A_\rho + h'} \left(1 + h'\varepsilon_3^p\right) \left[1 - \left(1 + h'\varepsilon_3^p\right)^{-\left(A_\rho/h'+1\right)}\right] \tag{36}$$

It can be denoted as σ_3^∞ when plastic strain is very large. Eq. (36) is approximatively described as

$$\sigma_3^\infty = \sum_{\rho=1}^{3} \frac{R_\rho}{A_\rho + h'} \left(1 + h'\varepsilon_3^p\right) \tag{37}$$

Let

$$E_t = \frac{\mathrm{d}\sigma_3^\infty}{\mathrm{d}\varepsilon_3^\infty} = \sum_{\rho=1}^{3} \frac{R_\rho h'}{A_\rho + h'} \tag{38a}$$

$$\sigma_0^\infty = \sigma_3^\infty\left(\varepsilon_3^p = 0\right) = \sum_{\rho=1}^{3} \frac{R_\rho}{A_\rho + h'} \tag{38b}$$

E_t and σ_0^∞ can be determined by using the linear segment of the corresponding experimental curve. Then h' can be obtained from Eq. (38). Fitting the deflection between $\sigma_3' = \sigma_0^\infty + E_t\varepsilon_3^p$ and the corresponding experimental value with the three terms power function, the constants A_1, A_2 and A_3 are obtained by comparing it and the second term on the right hand side of Eq. (36). The constant C_0 is obtained from Eq. (34) again.

According to the hypothesis (Watanabe and Atluri, 1986b), there has $\mathrm{d}f/\mathrm{d}L\big|_{L=0} \approx \mathrm{d}f'/\mathrm{d}L\big|_{L=0}$. Hence h can be determined as

$$h = h'/(C_0 - 1) \tag{39}$$

(2) The determination of constants associated with plastic delay angle θ (d_1, d_2, d_3, d_4, B_1, B_2, m) Choose a plastic strain path consisted of three linear segments shown in Fig. 10. The length of second segment is longer than the saturated length. One of the turning angle $|\alpha|$ is larger than 90° and the other is less than 90°, then carry out the experiments. Using these experimental data and $f(L)$ determined in (1) of this section, constants d_1, d_2, B_1 and B_2 in Eq. (20) can be obtained. Similarly, constants d_3, d_4 and m in Eq. (22) can be obtained by appropriate experiments.

4.2. Comparison of theoretical and experimental results

The material constants of 1Cr18Ni19Ti stainless steel material, determined with the above method, are shown in the Table 2.

Using Eqs. (20), (21), (22), (25), (26) and (27), some experiments with different plastic strain paths are simulated. Figs. 11–14 show our theoretical results and the experimental results. The results calculated by Valanis's model [let $\theta = \kappa = 0$ in Eq.

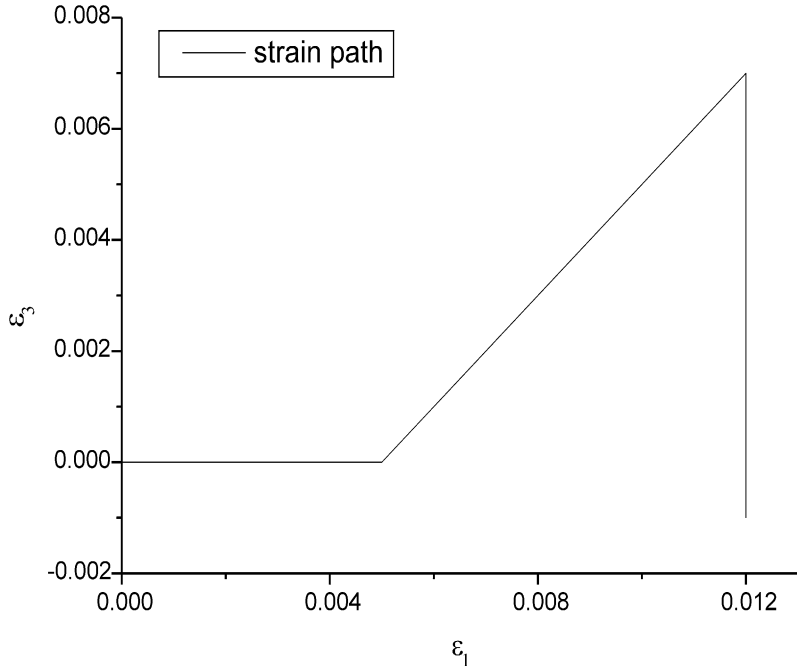

Fig. 10. Deformation path of three-segment linear path.

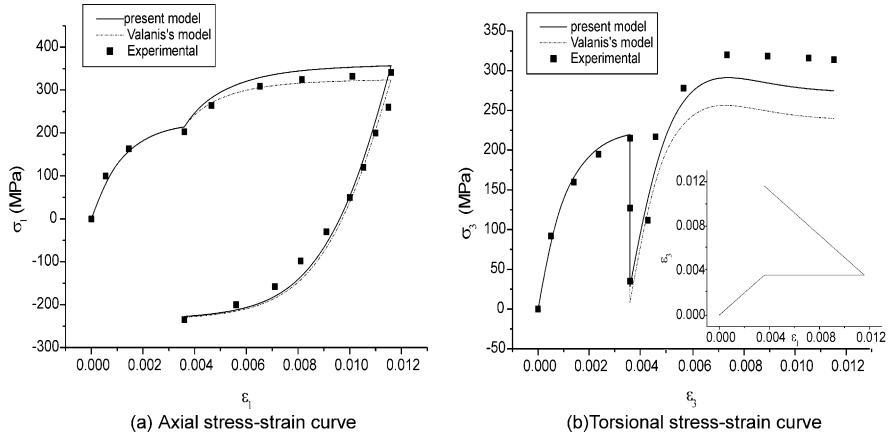

Fig. 11. Curve of stress response; (a) axial stress–strain curve, (b) torsional stress–strain curve.

(26)] are also drawn in Figs. 11 and 12. The loading paths in Figs. 11–14 are also shown at their own bottom.

Figs. 11 and 12 give the response curves of stress and strain of 1Cr18Ni19Ti stainless steel under axial-torsional combined loading along three-segment linear strain paths. Figs. 11(a), 12(a), 11(b) and 12(b) show the curves of axial stress versus

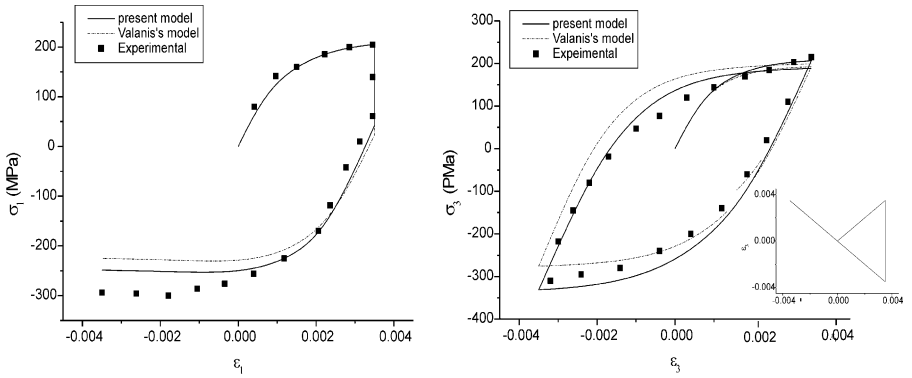

(a) Axial stress-strain curve (b) Torsional stress-strain curve

Fig. 12. Curve of stress response; (a) axial stress–strain curve, (b) torsional stress–strain curve.

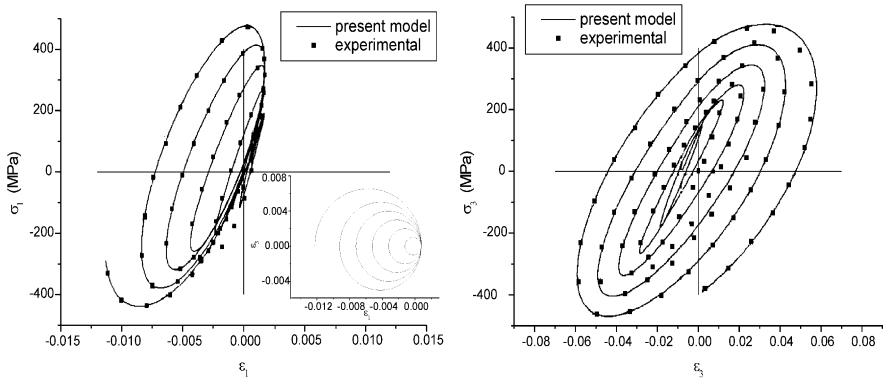

(a) Axial stress-strain curve (b) Torsional stress-strain curve

Fig. 13. Curve of stress response; (a) axial stress–strain curve, (b) torsional stress–strain curve.

strain $\sigma_1-\varepsilon_1$ and torsional stress versus strain $\sigma_3-\varepsilon_3$ for two different paths respectively. In the first loading segment of Figs. 11 and 12, the calculated results of present model and Valanis's model are coincided due to proportional loading. From Figs. 11 and 12(a and b), it is obvious that the predictions of the present model are close to the experimental results better than that calculated from Valanis's model in

Table 2
Material constants of 1Cr18Ni19Ti

A_1	A_2	A_3	R_1/MPa	R_2/MPa	R_3/MPa	C_0	h
875.0	850.3	5196.2	104249.9	49128.3	653362.5	1.2	20.0
	m	d_1	d_2	d_3	d_4	B_1	B_2
	0.61	0.21	0.28	26.0	0.179	4.014	308.2

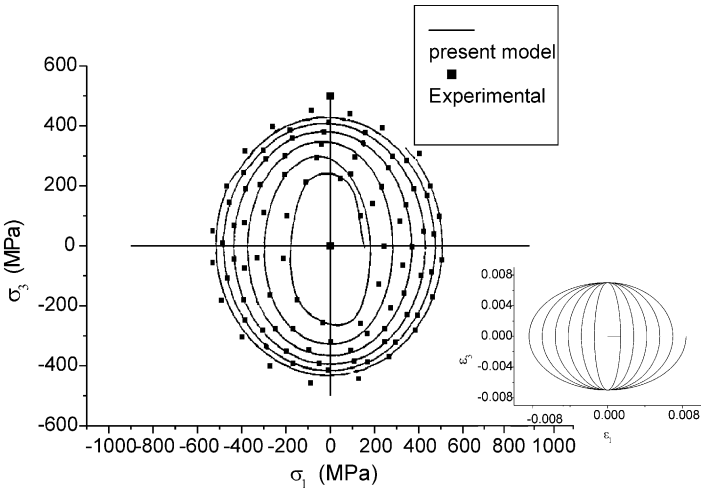

Fig. 14. Curve of stress response.

other two loading segments. Figs. 13 and 14 show the response curves of stress versus strain, along circular strain path with variational curvatures and elliptical strain path with different ratio of major axis to minor axis respectively. From Figs. 13(a and b) and 14, it is also seen that the theoretical results are close to that of experiments.

5. Biaxial ratcheting

Ratcheting phenomenon is that plastic strain will be accumulated in the direction of nonzero mean stress in a stress cycle (Shiratori et al., 1979; Hassan et al., 1992, Hassan and Kyrialides, 1992; Jiang and Sehitoglu, 1994a,b). Ratcheting behavior, which should be considered in the prediction of the structure life, is a basic phenomenon of the plastic cyclic. Many authors have researched uniaxial and multiaxial ratcheting (Chaboche, 1991; Ohno and Wang, 1993; McDowell, 1995; Jiang and Sehitoglu, 1996a,b; Ohno, 1997; Voyiadjis and Basuroychowdhury, 1998; Bari and Hassan, 2000, 2001, 2002). In this paper, we only simulate the biaxial (axial-torsional) ratcheting of the 316 stainless steel (Shiratori et al., 1979). In this experiment, first the thin-walled specimen is subjected to a constant pre-stress $\sigma_d = 67.4$

Table 3
Material constants of 316 stainless steel

A_1	A_2	A_3	R_1/MPa	R_2/MPa	R_3/MPa	C_0	h
827.2	805.4	5021.0	94310.3	44131.2	632292.7	1.8	21.0

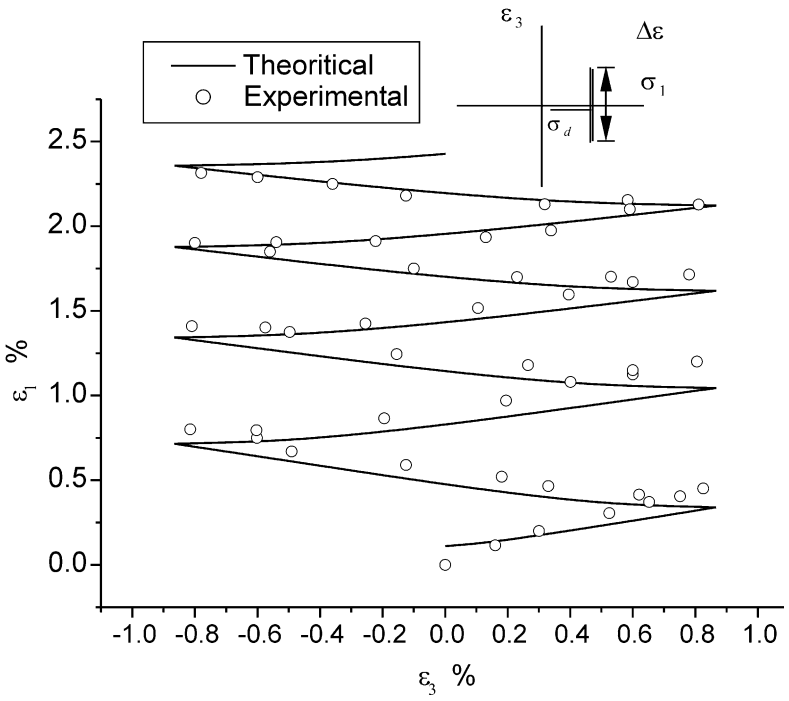

Fig. 15. Model comparison with experimental non-proportional ratcheting.

MPa, then subjected to torsional strain with the total strain amplitude $\Delta\varepsilon = 1\% = \Delta\gamma/\sqrt{3}$.

For biaxial ratcheting of the 316 stainless steel only 8 material constants should be considered due to that the constants related to θ are almost zero. The constants are determined with the previous method and shown in the Table 3.

The plastic strain accumulation due to nonzero mean stress is shown in Fig. 15. The theoretical result, by using Eqs. (26) and (27), shows that there is a strain accumulation in the direction of nonzero mean stress and no strain accumulation in other direction, which is agreement with the experimental results. Comparing the present result with that of Basuroychowdhury and Voyiadjis (1998), it is found that the present model with a small amount of parameters gives a better prediction. It is also found that the prediction is good agreement with experimental result in initial several cycles, but there is an obvious deviation after large cycles due to that ratcheting is very complex. The further research is necessary.

6. Conclusions

A new elasto-plastic integral constitutive model is developed in this paper to simulate a number of axial-torsional experiments. In the present constitutive model, stress is expressed as a functional of the intrinsic geometry parameters of plastic

strain trajectory and material behavior. Owing to fully introducing the intrinsic geometry parameters (plastic strain arc-length, endochronic, curvature and characteristic points), the plastic deformation history can be modeled in a satisfactory way. The developed model has the capability to describe responses in complex loading cases. The simulated results on 1Cr18Ni19Ti stainless steel under axial-torsional combined loading show a good agreement with the experimental results. Moreover, the biaxial ratcheting response on the 316 stainless steel is simulated with this model, which also gives a better prediction. This integral constitutive theory is compatible with classical plastic theory, but the former is more flexible in practical application and the amount of calculation work is little when parameters are determined.

Acknowledgements

This work is supported by the National Natural Science Foundation through Grants No. 10132010 and 10072033.

References

Armstrong, P.J., Frederick, C.O., 1966. A Mathematical Representation of the Multiaxial Bauschinger Effect. CEGB Report RD/B/N731. Central Electricity Generating Board.

Bari, S., Hassan, T., 2000. Anatomy of coupled constitutive models for ratcheting simulation. International Journal of Plasticity 16, 381–409.

Bari, S., Hassan, T., 2001. Kinematic hardening rules in uncoupled modeling for multiaxial ratcheting simulation. International Journal of Plasticity 17 (7), 885–905.

Bari, S., Hassan, T., 2002. An advancement in cyclic plasticity modeling for multiaxial ratcheting simulation. International Journal of Plasticity 18 (7), 873–894.

Basuroychowdhury, I.N., Voyiadjis, G.Z., 1998. A multiaxial cyclic plasticity model for non-proportional loading cases. International Journal of Plasticity 14 (9), 855–870.

Besseling, J.F., 1958. A theory of elastic, plastic and creep deformations of an initially isotropic material showing anisotropic strain hardening, creep recovery and secondary creep. ASME Journal of Applied Mechanics 25, 529–536.

Bodner, S.R., Partom, Y., 1972. A large deformation elastic-viscoplastic analysis of a thick-walled spherical shell. ASME Journal of Applied Mechanics 39, 751–757.

Celentano, D.J., 2001. A large strain thermoviscoplastic formulation for the solidification of S.G. Cast iron in a green sand mould. International Journal of Plasticity 17 (12), 1623–1658.

Chaboche, J.L., 1977. Viscoplastic constitutive equations for the description of cyclic and anisotropic behavior of metals. Bull. Acard. Polon. Sci. Ser. Sci. Technol. 25, 33–42.

Chaboche, J.L., 1991. On some modifications of kinematic hardening to improve the description of ratchetting effects. International Journal of Plasticity 7, 661–678.

Dafalias, Y.F., Popov, E.P., 1975. A model of nonlinearly hardening materials for complex loading. Acta. Mech. 21, 173–192.

Dewel, G., et al., 1981. Layered structers in two dimensional nonequilibrium system. J. Phys. Lett. (Paris) 42, L361–L364.

Drucker, D.C., 1950. Some implications of Work-hardening and ideal plasticity. Quarterly Journal of Applied Mechanics 7, 411–418.

Hashiguchi, K., 1988. A mathematical modification of two surface model formulation in plasticity. Int. J. Solids Struct. 24, 987–1001.

Hashiguchi, K., Tsutsum, S., 2001. Elastoplastic constitutive equation with tangential stress rate effect. International Journal of Plasticity 17 (1), 117–145.
Hassan, T., Cornoa, E., Kyrialides, S., 1992. Ratcheting in cyclic plasticity, part II:multiaxial behavior. International Journal of Plasticity 8, 117–146.
Hassan, T., Kyrialides, S., 1992. Ratcheting in cyclic plasticity, part I:unaxial behavior. International Journal of Plasticity 8, 91–116.
Hill, R., 1950. The Mathematical Theory of Plasticity. Oxford University Press, Oxford.
Ilyushin, A.A., 1954. On the relation between tresses and small strains in continuum mechanics. Prikl. Mat and Mekh. 18, 641–666 (in Russian).
Ilyushin, A.A., 1963. Plasticity. Izd. Akad. Nauk. SSSR, Moscow.
Jiang, Y., Sehitoglu, H., 1994a. Multiaxial cyclic ratcheting under multiple step Loading. International Journal of Plasticity 10 (8), 849–870.
Jiang, Y., Sehitoglu, H., 1994b. Cyclic ratchetting of 1070 steel under multiaxial stress states. International Journal of Plasticity 10 (5), 579–608.
Jiang, Y., Sehitoglu, H., 1996a. Modeling of cyclic ratchetting plasticity, part I: development of constitutive relations. Journal of Applied Mechanics 63, 720–725.
Jiang, Y., Sehitoglu, H., 1996b. Modeling of cyclic ratchetting plasticity, part, part II: comparison of model simulations with experiments. Journal of Applied Mechanics 63, 726–733.
Jiang, Y., Kurath, P., 1997. Nonproportional cyclic deformation: critical experimental and analytical modeling. International Journal of Plasticity 13 (8-9), 743–763.
Kaneko, K., Oyamada, T., 2000. A viscoplastic constitutive model with effect of aging. International Journal of Plasticity 16 (3-4), 337–358.
Krempl, E., McMaho, J.J., Yao, D., 1986. Viscoplasticity based on overstress with a differential growth law for the equilibrium stress. Mech. Mats. 35–48.
Krieg, R.D., 1975. A practical two surface plasticity theory. ASME Journal of Applied Mechanics 42, 641–646.
Kuang, Z.B., 1989. Foundation of non-linear continuum medium mechanics. Xi'an Jiaotong University Press, Xi'an (in Chinese).
Kuang, Z.B., 1990. Integral Constitutive Equations of Elasto-Plastic Materials. Acta Mechanics Solids Sinica 3, 245–263.
Kuang, Z.B., 2002. Continuum Mechanics. Shanghai Jiaotong University Press, Shanghai (in Chinese).
Lensky, V.S., 1962. Local hypothesis in the theory of plasticity. Izv. Akad. Nauk SSSR, Otd. Tekh. Nauk. Mekh. Mashinostrenie 5, 154–158.
Lion, A., 2000. Constitutive modelling in finite thermoviscoplasticity: a physical approach based on nonlinear rheological models. International Journal of Plasticity 16 (5), 469–494.
Mahler, L., Ekh, M., Runesson, K., 2001. A class of thermo-hyperelastic-viscoplastic models for porous materials: theory and numerics. International Journal of Plasticity 17 (7), 943–969.
Marquis, D., 1979. Modelisation et Identification de I'Ecrouissage Anisotrope Desmetaux. These Paris VI.
Mashkov, I.D., 1970. Mekh. Tverdogo.te.la 4, 191–195.
McDowell, D.L., 1995. Stress state dependence of cyclic ratcheting behavior of two rail steel [J]. International Journal of Plasticity 11 (4), 397–421.
Miller, A., 1976. An inelastic constitutive model for monotonic, cyclic and creep deformation. ASME J. Eng. Mater. Technol. 98, 97–113.
Mroz, Z., 1967. On the description of anisotropic work hardening. J. Mech. Phys. Solid 15, 163–175.
Mughrabi, H., et al., 1979. Fatigue Mechanisms. ASTM675,69.
Naghdi, P.M., Trapp, J.A., 1975. The significance of formulating plasticity theory with reference to loading surfaces in strain space. Int. J. Engng. Sci. 13, 785–797.
Ohashi, Y., Tokuda, M., 1973. Precise measurement of plastic behavior of mild steel tubular specimens subjected to combined torsion and axial force. J. Mech. Phys. Solid 21, 241–261.
Ohno, N., 1982. A constitutive model of cyclic plasticity with a nonhardening strain region. ASME Journal of Applied Mechanics 49, 721–727.
Ohno, N., Wang, J., 1991. Transformation of a nonlinear kinematic hardening rule to a multisurface form under isothermal and nonisothermal conditions. International Journal of Plasticity 7 (8), 879–891.

Ohno, N., Wang, J.D., 1993. Kinematic hardening rules with critical state of dynamic recovery, part I: formulations and basic features for ratcheting behavior. International Journal of Plasticity 9, 375–390.
Ohno, N., 1997. Constitutive modeling of cyclic plasticity with emphasis on ratchetting. Int. J. Mech. 40, 251–261.
Pipkin, A.C., Rivlin, R.S., 1965. Mechanics of rate-independent materials. ZAMP 16 (3), 313–327.
Prager, W., 1955. The Theory of Plasticity: A Survey of Recent Achievements, James Clayton Lecture. Proc. Institution of Mechanical Engineers, London. vol. 169, pp. 41–50.
Rousselier, G., Engel, J.J. and Manson, J.C., 1985. Etude Comparative de Modeles de Comportment Pour la Simulation d'Essais en Traction-Compression sur Tubes en Acier Inoxydable. Document EDF-DER, annexe du Rapport No.8 du GIS Rupture a Chand.
Shevchenko, Y.N., Babeshko, M.E., 1990. Determining equations of deformational type describing the thermoelastoviscoplastic processes of deformation of material along plane trajectories. Prikl. Mekh. 26, 38–44.
Shiratori, E., Ikegami, K., Yoshida, F., 1979. Analysis of stress-strain relations of use of an anisotropic hardening potential. J. Mech. Physics Solids 27, 213–229.
Valanis, K.C., 1971. A theory of viscoplasticity without a yield surface. Arch. Mech. 23, 517–551.
Valanis, K.C., 1980. Fundamental consequences of a new intrinsic time measure plasticity as a limit of the endochronic theory. Arch. Mech. 32, 171–191.
Voyiadjis, G.Z., Thiagarajan, G., 1996. A cyclic anisotropic-plasticity model for metal matrix composites. International Journal of Plasticity 12 (10), 69–92.
Voyadjis, G.Z., Basuroychowdhury, I.N., 1998. A plastici model for multiaxial cyclic loading and ratcheting. Acta Mechanic 126, 19–35.
Walker, K.P., 1981. Research and Development Program for Nonlinear Structural Modeling with Advanced Time-Temperature Dependent Constitutive Relationships, NASA CR-165533, NASA.
Wang, H., Barkey, M.E., 1999. A strain space nonlinear kinematic hardening/softening plasticity model. International Journal of Plasticity 15 (7), 755–778.
Watanabe, O., Atluri, S.N., 1986a. Internal time, general internal variable and multi-yield-surface theories of plasticity and creep: a unification of concepts. International Journal of Plasticity 2, 37–57.
Watanabe, O., Atluri, S.N., 1986b. Constitutive modeling of cyclic plasticity and creep using an internal time concept. International Journal of Plasticity 2, 107–134.
Xiao, L., Kuang, Z.B., 1998. The macroscopical responses and microcosmic structure of Zr-4 alloy under non-proportional loading. Acta Metal Sinica 34, 242–248.
Yanagida, N., Watanabe, O., 1991. An approach of material-constant determination for internal time theory in arbitrary cyclic plasticity. The 1st JSME/ASME Joint International Conference on Nuclear engineering, Vol. 1, pp. 541–547.
Yoshida, F., 2000. A constitutive model of cyclic plasticity. International Journal of Plasticity 16 (3-4), 359–381.
Zbib, H., Rubia, T.D., 2002. A multiscale model of plasticity. International Journal of Plasticity 18 (9), 1133–1163.
Zhao, S.X., Kuang, Z.B., 1996a. An elasto-plastic constitutive equation for the stainless steel under Combined axial and torsional loads part I: experiment. Acta Mechanic Sinica 28 (4), 412–420.
Zhao, S.X., Kuang, Z.B., 1996b. An elasto-plastic constitutive equation for the stainless steel under Combined axial and torsional loads part: II theory. Acta Mechanic Sinica 28 (6), 745–750.
Zhou, Z., Kuang, Z.B., 1999. A study on the elasto-plastic mechanical behavior of two-phase media under non-proportional loading. Acta Mechanic Sinica 31 (2), 185–192.
Zubchaninov, V.G., 1991. Constitutive relations for elasto-plastic processes. Soviet Applied Mechanics 27 (3), 1143–1152.